

Article

Alkaline-Activation Technique to Produce Low-Temperature Sintering Activated-HAp Ceramic

Wan Mohd Arif W. Ibrahim ^{1,2,*} , Mohd Mustafa Al Bakri Abdullah ^{2,*}, Noorina Hidayu Jamil ³, Hasmaliza Mohamad ⁴, Mohd Arif Anuar Mohd Salleh ², Andrei Victor Sandu ^{5,6,7,*} , Petrica Vizureanu ^{5,8} , Madalina Simona Baltatu ⁵  and Patimapon Sukmak ⁹ 

- ¹ Center of Excellence Geopolymer and Green Technology (CEGeoGTech), Universiti Malaysia Perlis (UniMAP), Arau 02600, Perlis, Malaysia
 - ² Faculty of Chemical Engineering & Technology, Universiti Malaysia Perlis (UniMAP), Arau 02600, Perlis, Malaysia
 - ³ Faculty of Mechanical Engineering & Technology, Universiti Malaysia Perlis (UniMAP), Arau 02600, Perlis, Malaysia
 - ⁴ School of Materials and Mineral Resources Engineering, Universiti Sains Malaysia, Gelugor 11800, Penang, Malaysia
 - ⁵ Faculty of Material Science and Engineering, Gheorghe Asachi Technical University of Iasi, 41 D. Mangeron St., 700050 Iasi, Romania
 - ⁶ Romanian Inventors Forum, Str. Sf. P. Movila 3, 700089 Iasi, Romania
 - ⁷ National Institute for Research and Development for Environmental Protection INCDPM, 294 Splaiul Independentei, 060031 Bucharest, Romania
 - ⁸ Technical Sciences Academy of Romania, Dacia Blvd 26, 030167 Bucharest, Romania
 - ⁹ Center of Excellence in Sustainable Disaster Management, School of Engineering and Technology, Walailak University, Nakhonsithammarat 80161, Thailand
- * Correspondence: wmarif@unimap.edu.my (W.M.A.W.I.); mustafa_albakri@unimap.edu.my (M.M.A.B.A.); sav@tuiasi.ro (A.V.S.)



Citation: Ibrahim, W.M.A.W.; Abdullah, M.M.A.B.; Jamil, N.H.; Mohamad, H.; Salleh, M.A.A.M.; Sandu, A.V.; Vizureanu, P.; Baltatu, M.S.; Sukmak, P. Alkaline-Activation Technique to Produce Low-Temperature Sintering Activated-HAp Ceramic. *Appl. Sci.* **2023**, *13*, 2643. <https://doi.org/10.3390/app13042643>

Academic Editor: Asterios Bakolas

Received: 19 December 2022

Revised: 16 February 2023

Accepted: 17 February 2023

Published: 18 February 2023



Copyright: © 2023 by the authors. Licensee MDPI, Basel, Switzerland. This article is an open access article distributed under the terms and conditions of the Creative Commons Attribution (CC BY) license (<https://creativecommons.org/licenses/by/4.0/>).

Abstract: The fabrication of hydroxyapatite (HAp) ceramics prepared by existing conventional sintering requires high-temperature sintering of 1250 °C to 1300 °C. In this paper, the activated metakaolin (MK)/HAp specimens were prepared from varied mix design inputs, which were varied solid mixtures (different amounts of MK loading in HAp) and liquid-to-solid (L/S) ratios, before being pressed and sintered at 900 °C. Phase analysis, thermal analysis, surface morphology, and tensile strength of the specimens were investigated to study the influences of the Al, Si, Fe, Na, and K composition on the formation of the hydroxyapatite phase and its tensile strength. XRD analysis results show the formation of different phases was obtained from the different mix design inputs HAp (hexagonal and monoclinic), calcium phosphate, sodium calcium phosphate silicate and calcium hydrogen phosphate hydrate. Interestingly, the specimen with the addition of 30 g MK prepared at a 1.25 L/S ratio showed the formation of a monoclinic hydroxyapatite phase, resulting in the highest diametrical tensile strength of 12.52 MPa. Moreover, the increment in the MK amount in the specimens promotes better densification when sintered at 900 °C, which was highlighted in the microstructure study. This may be attributed to the Fe₂O₃, Na₂O, and K₂O contents in the MK and alkaline activator, which acted as a self-fluxing agent and contributed to the lower sintering temperature. Therefore, the research revealed that the addition of MK in the activated-HAp system could achieve a stable hydroxyapatite phase and better tensile strength at a low sintering temperature.

Keywords: alkali-activated-hydroxyapatite; hydroxyapatite phase; diametrical tensile strength; monoclinic

1. Introduction

Over the past four decades, there has been a major advance in the development of medical materials, and this includes the innovation of ceramic materials for skeletal repair and reconstruction [1]. These so-called “bio-ceramic materials”, which are known for their

biocompatibility [2], bioinert, and bioactive [3], are a special kind of biomaterial that is used to treat, augment, repair, or replace the diseased or damaged hard tissue of the human body [3,4]. There is currently widespread research being conducted in the development of bio-ceramic materials; such studies are motivated not only by the beneficial technical properties of the materials such as phase stability and bioactivity but also by the potential to reduce energy consumption in the fabrication of bio-ceramic products [5] that are also effective in their action, minimizing the process and being economical [6]. Other research additionally incorporated bio-ceramic material with other materials such as an iron oxide to improve the synthesis methods to produce the HAp with a magnetic core [7]. Hence, in order to reduce energy consumption during the fabrication of bio-ceramics, there is a need to explore a new technique to ensure that the densification of ceramic materials can be achieved at lower sintering temperatures.

Among the various forms of bioceramics, calcium phosphate, particularly hydroxyapatite ($\text{Ca}_{10}(\text{PO}_4)_6(\text{OH})_2$; HAp), has received great attention due to its chemical and crystallographic structure which has similar mineral components to those of bones and teeth of vertebrates [8–11]. Furthermore, HAp is resistant to X-ray radiation and UV irradiation without visible aging and structural damage that may be implied in certain clinical treatments [12,13]. Kroczek et al. summarize the current knowledge of HAp in medicine and dentistry from the perspective of their use in the manufacture of transitional implants for guided bone regeneration [14] and their works have also been supported by other researchers [15–17]. Meanwhile, HAp nanoparticles have become a matter of interest in biomedical research not only in bone management but also in the development of cancer drug delivery systems [18–20] as well as in future perspectives in cosmetics and oral care products [21,22].

In addition, research conducted in the past has shown that the pure HAp of high crystallinity can be replicated through conventional sintering techniques [23]. The densification of hydroxyapatite is highly dependent on the sintering temperature, and the optimized sintering temperature is commonly reported within the range of 1200–1300 °C [24–28]. However, HAp tends to decompose at this high temperature. A previous study reported that the phase transformation which occurs at high sintering temperatures will finally lead to the formation of α -tricalcium (α -TCP) and calcium oxide at 1400 °C, accompanied by a nanopore formation. The nanopores that disperse in the α -TCP grains are the main factor leading to low density and decreased mechanical strength of the specimens [29]. Meanwhile, research conducted at low sintering temperatures of ~800 °C exhibited slow dihydroxylation behavior and promoted low densification resulting in poor mechanical properties [30].

In order to maintain the conventional sintering technique in producing HAp ceramics at a lower sintering temperature, a new approach to activate the HAp with alkaline activation prior to the sintering process could be considered. This process is called “geopolymerization”. A previous study has shown that sintered kaolin ceramics at 900 °C can be achieved by initiating the geopolymerization and that this results in a good performance of compressive strength [31]. Besides the good performance on mechanical properties of the sintered activated-ceramic product that can be achieved, the geopolymerization that uses kaolin/metakaolin as a source of alkali-activated materials (AAM) also exhibited good bioactivity of the products [32,33].

The geopolymerization process is characterized by the following stages: (1) dissolution of oxide minerals from alumina–silica-rich source materials under high alkaline conditions; (2) transport/orientation of dissolved oxide minerals followed by gelation; and (3) polycondensation to form a stable 3D network of a silicoaluminate structure. Numerous aspects influence the geopolymerization process, including the chemical and mineralogical composition of the starting materials, curing temperature, water content, and alkaline component concentration [31]. To obtain the reactive or amorphous phase required for the geopolymerization reaction, thermally heated kaolinite clay in the range of 550–850 °C remains the primary source of metakaolin. The amount of reactive SiO_2 and Al_2O_3 in the

produced metakaolin is dependent on the purity of the kaolin clay used as the starting material [34]. In previous work, metakaolin-based geopolymer with up to 30 wt% quartz sand was found to be more compact, exhibited less drying shrinkage, and possessed greater mechanical strength than the specimen without quartz [35]. In medical applications, kaolin has, over time, been used as an additive, adsorbent, and agent for blood clotting because it enables charge interactions with clotting factors, besides having huge potential to accelerate haemostasis. Kaolin was reported to be mechanically reliable, in addition to its non-toxicity [36].

Sintering of geopolymers always results in the formation of sintered ceramic bodies with improved properties [31,37–39]. A particular procedure is required in order to manage the purity, particle size, particle size distribution, and heterogeneity of ceramic products which employ naturally occurring rock sand minerals as the raw materials. These parameters have a substantial impact on the ultimate qualities of ceramics. The process of the sintering reaction is affected by impurities and the mineralogical structure of the kaolin minerals. Extrusion, slip casting, pressing, tape casting, and injection molding are the most popular techniques used to produce a green body prior to further heat treated to form a rigid, final product. Conventional sintering remains a popular method for HAp ceramic fabrication due to its simplicity. However, it still struggles to preserve their compatibility and prevent the degradation of the HAp structure during the high-temperature sintering.

The objective of this research was to identify the effect of the mix design input on the preparation of a low sintering temperature of MK/HAp bioceramics. This will lead to an understanding of the chemical composition, which may act as a self-fluxing agent during geopolymerization, and thus its contribution to the phase stability and mechanical property.

2. Materials and Methods

2.1. Materials

Several starting materials were used in the formulation of the alkaline activated-hydroxyapatite (MK/HAp) bio-ceramic which are: hydroxyapatite (HAp), kaolin, sodium hydroxide (NaOH), sodium silicate (Na_2SiO_3) pallets, and water. High-purity HAp powder (heavy metals ≤ 20.0 ppm) with a particle size of $10 \mu\text{m}$ was obtained from Sigma-Aldrich, St. Louis, MO, USA, and free-flow grade kaolin powder was additionally obtained from Sigma-Aldrich, USA. Both were used in the form as received in this study. Metakaolin (MK), the primary precursor material of the geopolymerization, was obtained by the calcination of the raw kaolin at 750°C for three hours in the air, using an electric oven. The NaOH used in this study is type Formosa-P from the Formosa Plastic Corporation, Taipei, Taiwan with 99.0 % purity. In addition, the Na_2SiO_3 used was obtained from South Pacific Chemicals Industries Sdn. Bhd. (SPCI), Selangor, Malaysia.

2.2. Preparation of MK/HAp Bio-Ceramic

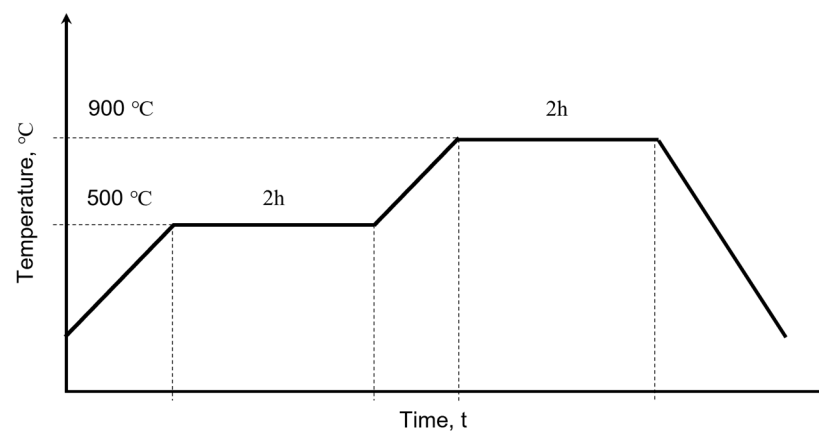
In total, nine mix designs of activated MK/HAp were prepared, and details of the design inputs are shown in Table 1. Initially, MK/HAp was activated using the geopolymerization technique. For the solid part, 10 g, 20 g, and 30 g of metakaolin were added to the 100 g of HAp for the ball-milling. The milling process was performed in a PTFE mill jar with ZrO_2 balls using a customized lab roll ball mill (Ultraform Engineering, Bayan Lepas, Malaysia; 0–570 rpm rotation speed) at 200 rpm for three hours in dry conditions. The alkaline solution used for geopolymerization was obtained by mixing 8 M of NaOH solution with sodium silicate solution in the volume proportion of 1:2. The mix solution was cooled and kept at room temperature for 24 h before use.

Table 1. Mix design inputs used in the experiment.

Mix	Solid		Liquid (1:2)			L/S Ratio	Curing Condition	
	Hap (g)	MK (g)	Total Solid (g)	8 M NaOH (g)	Na ₂ SiO ₃ (g)			Total Liquid (g)
HM10-1.00	100	10	110	36.67	73.33	110.00	1.00	60 °C/2 d
HM10-1.25	100	10	110	45.83	91.67	137.50	1.25	60 °C/2 d
HM10-1.50	100	10	110	55.00	110.00	165.00	1.50	60 °C/2 d
HM20-1.00	100	20	120	40.00	80.00	120.00	1.00	60 °C/2 d
HM20-1.25	100	20	120	50.00	100.00	150.00	1.25	60 °C/2 d
HM20-1.50	100	20	120	60.00	120.00	180.00	1.50	60 °C/2 d
HM30-1.00	100	30	130	43.33	86.67	130.00	1.00	60 °C/2 d
HM30-1.25	100	30	130	54.17	108.33	162.50	1.25	60 °C/2 d
HM30-1.50	100	30	130	65.00	130.00	195.00	1.50	60 °C/2 d

In preparing the MK/HAp paste, the raw materials were made by manually mixing the alkaline solution with the mixture of MK and HAp powder using three different liquid-to-solid ratios (L/S ratio—1.00, 1.25 and 1.50). The activated specimens were then dried in the oven at 60 °C for two days in order to obtain completely dried specimens prior to ceramic body fabrication. However, the mix design input of HM30-1.00 prepared at an L/S ratio of 1.00 could not be achieved because of its poor workability during mixing; thus, it has not proceeded for further specimen preparation. This was due to the low liquid content being insufficient to activate the highest metakaolin addition of the specimens.

The dried MK/HAp specimens were crushed into small pieces with the use of a mortar grinder followed by a dry milling process at 300 rpm for 48 h performed in PTFE mill jar with ZrO₂ balls. The powder was subsequently sieved through a 63 µm stainless steel test sieve prior to the compaction process. The compression operation was performed using an Atlas Manual 15T hydraulic hand press (Specac Ltd., Orpington, UK) at 40 MPa for two minutes, yielding green compacts with a diameter of 15 mm and a thickness of approximately 5 mm. MK/HAp bio-ceramics were obtained by the two-step sintering method (Figure 1) using a Carbolite ELF 11/148 chamber furnace (Carbolite, Hope Valley, UK). During the first step operation, the sample is heated up at 3 °C/min to 500 °C for two hours; this was designed to burn out the organic compound from the alkali activator and to promote the densification of the green compacts. The second step was carried out using the same heating rate of 3 °C/min up to 900 °C for another 2 h of dwell time to obtain the respective MK/HAp bio-ceramic specimens.

**Figure 1.** Two-step sintering profile.

2.3. Physicochemical Characterization

The elemental composition analysis was carried out using the ARL Quant'X (Thermo Scientific Inc., Waltham, MA, USA) EDXRF spectrometer analyzer. The general chemical

composition of the starting materials obtained from the EDXRF spectrometer analyzer is presented in Table 2. The oxide ratio of Ca:P is 3.29 while the Si:Al ratios are found to be 1.41 and 1.52 for kaolin and metakaolin, respectively.

Table 2. Composition of HAp, kaolin and metakaolin.

Chemical Composition (Compound)	CaO	P ₂ O ₅	Al ₂ O ₃	SiO ₂	Na ₂ O	TiO ₂	Fe ₂ O ₃	MgO	K ₂ O
HAp	61.35	18.63	14.00	0.38	0.10	-	-	5.20	-
Metakaolin (MK)	-	-	38.70	59.00	0.40	1.10	0.60	-	0.10

The mineralogical analysis of the raw materials and activated HAp were determined by a Bruker D2 Phaser X-ray diffractometer (XRD) (Bruker, Germany) with Cu K α radiation (40 kV and 30 mA). Figure 2 shows the XRD patterns of kaolin, metakaolin, and hydroxyapatite. As can be seen, the XRD pattern of kaolin (Figure 2a) exhibits two prominent reflections at 12.33° and 24.90° 2 θ , and other reflections at 19.84°, 34.93°, 38.43°, and 55.11° 2 θ . These reflections were matched with the PDF card number 01-089-6538, as reported by Obada et al. [36]. The results indicate that kaolinite was the predominant phase in the powdery bulk. Heat-treated kaolin at 750 °C was converted into metakaolin, where the X-ray pattern showed a diffuse halo peak with 2 θ between 18–38° (Figure 2b), which is the characteristic of the amorphous phase as presented in metakaolin [40,41]. The main components of metakaolin were SiO₂ and Al₂O₃, although it contained roughly 1.10 wt% of TiO₂ as a major impurity which is identified as anatase in the XRD analysis [42]. Meanwhile, Figure 2c shows the XRD pattern of the raw HAp powder in which the pattern matched the hydroxyapatite phase as per PDF card number 00-009-0432 (25.85°, 31.71°, and 32.90° 2 θ) [43]. There was no apparent secondary phase observed from the pattern which determined the high purity of the HAp powder.

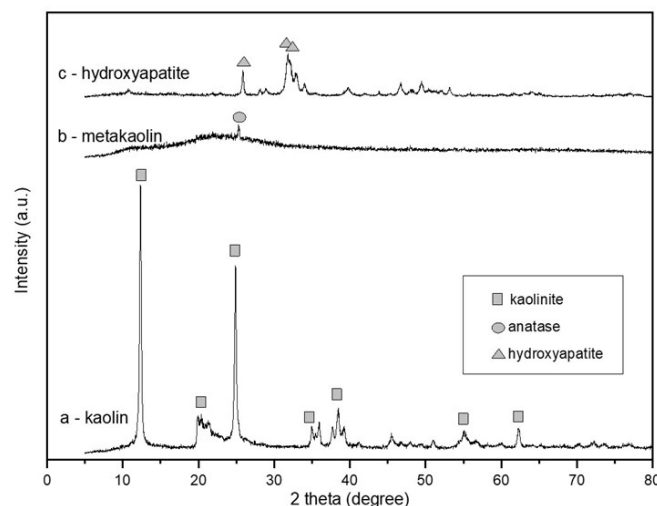


Figure 2. The XRD patterns of: (a) kaolin, (b) metakaolin, and (c) hydroxyapatite.

The Fourier transform infrared spectroscopy (FT-IR) measurement was carried out to confirm the dihydroxylation of water molecules after the heat treatment of raw kaolin. The test was conducted on an FT-IR analyzer (Perkin Elmer, Waltham, MA, USA) using normal potassium bromide (KBr) KBr pellets, and about 2 mg of the specimen was ground and pressed into disc form to evaluate the shifting of functional groups. The analyses were performed in the spectral range from 4000 to 400 cm⁻¹ and the number of scans was 60.

Figure 3 shows the FT-IR analysis of kaolin and metakaolin. The FT-IR spectra of kaolin showing the absorption bands at 3695–3621 cm⁻¹ expressed the stretching vibrations of -OH groups of kaolinite. The bands located at 3436 and 1631 cm⁻¹ corresponded,

respectively, to the stretching vibrations of water molecules, while those at 1190–1082 cm^{-1} and then at 1010 and 789 cm^{-1} expressed, respectively, the vibrations of the Si-O-Si and Si-O-Al groups of the network. The bands at 921 and 789 cm^{-1} indicated the presence of the stretching vibration of Al-OH where Al is in coordination with VI. The band at 542 cm^{-1} indicated the vibrations of the Si-O-Si and Si-O-Al groups of the network. Thermal treatment of kaolin generally causes its transformation to metakaolin. The FT-IR spectra of metakaolin confirmed the occurrence of kaolinite dihydroxylation during the heat treatment of kaolin, whereby no fingerprint bands at 3695–3621 cm^{-1} were observed on the spectra; contrarily, the metakaolin spectra were mainly characterized by the 1065 cm^{-1} band which corresponded to the stretching vibration of the Si-O-Si and Si-O-Al groups of the metakaolin network [40].

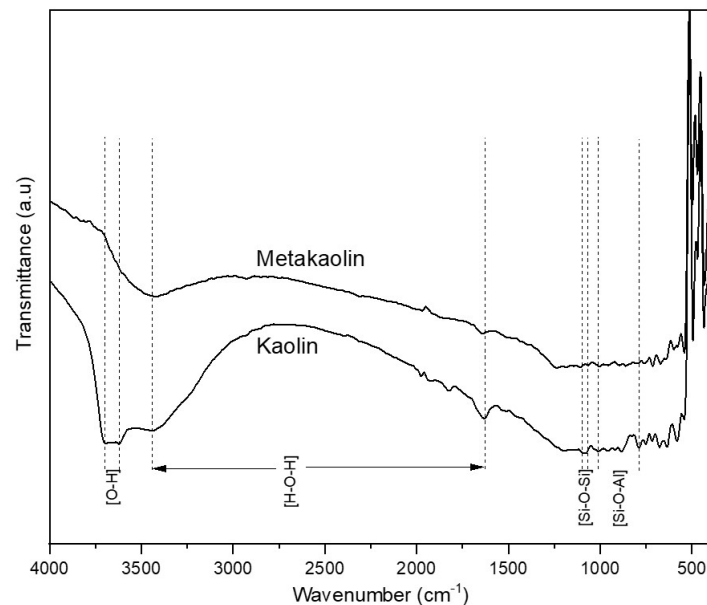


Figure 3. FT-IR spectra of kaolin and metakaolin.

The thermogravimetric analysis (TGA) was conducted to observe the mass loss during heating. The heating rate was maintained at 2 °C per minute using TGA/DSC 2 HT Mettler Toledo (Columbus, OH, USA), and the testing was done up to the temperature of 1200 °C.

The morphology of the specimens was obtained from various locations on the as-sintered specimens using a Vega Tescan scanning electron microscope (SEM) (Tescan, Brno, Czech Republic) equipped with energy-dispersive X-ray spectroscopy (EDS). The analysis of the tensile strength was performed on the sintered specimens in the form of cylindrical pallets (15 mm in diameter and 5 mm in height) in accordance with ASTM C 496. The diametral tensile strength (DTS) values were measured on three specimens from each mix design input using a Shimadzu, AG-X Plus universal testing machine (Shimadzu, Kyoto, Japan). The crosshead speed was 0.600 mm/min. The DTS values were calculated using Equation (1):

$$\sigma = \frac{2F}{\pi DT} \quad (1)$$

where:

σ = diametral tensile strength (DTS) [MPa],
 F = force causing the destruction of the specimen [N],
 D = diameter of the specimen [mm],
 T = thickness of the specimen [mm].

The mean value \pm standard deviation values of at least three independent specimens were used for obtaining all the results [44].

3. Results and Discussion

3.1. Phase Analysis

Figure 4 shows the XRD spectra for all the specimens compact sintered at 900 °C, including the as-received HAp as a reference. The patterns indicated the presence of well-crystallized phases in all specimens, where higher crystallinity is observed in the as-received HAp compared to others. No apparent structural transition or peak shifts occur in the specimen as-received HAp, HM10-1.00 and HM30-1.25, indicating a major HAp phase was present without apparent secondary phases. The HAp reference specimen and HM10-1.00 displayed main character peaks at 23.26°, 32.56°, 33.32°, and 47.06° 2θ, which correspond to the hexagonal structure of the hydroxyapatite phase (Powder Diffraction File-PDF No. 01-086-0740).

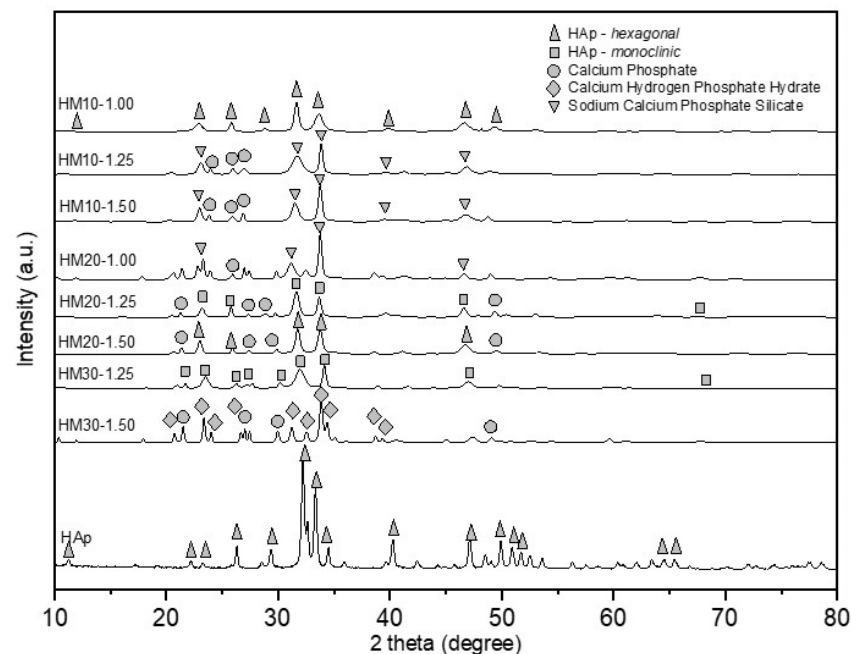


Figure 4. Phase diffractogram of mix design inputs of MK/HAp sintered at 900 °C.

HM30-1.25 specimen indicates the formation of the monoclinic HAp phase through the peak's determination at 23.49°, 31.95°, 34.12°, 46.98°, and 68.24° 2θ (Powder Diffraction File-PDF No. 01-089-4405) [45]. To better elucidate the formation of the monoclinic HAp and taking account that the XRD characteristic peaks (at dominant peaks) of this phase overlap with the hexagonal by geometric similarity, it was necessary to carry out thorough observations on the identification of the peaks at high angles (2θ) [45,46]. Reference peaks from the hexagonal HAp PDF Card indicate that no peaks can be observed within the 2θ range of 67° to 69°. However, peaks with lower intensity still can be observed within the 2θ range indicating the formation of a monoclinic structure. Figure 5 shows the magnified region of all HAp phase specimens, where HM20-1.25 and HM30-1.25 indicate the presence of a peak at 67.71° and 68.38° 2θ respectively. Sanchez [45] reported that 97% of the related scientific works observed that almost all the crystallographic analyses referring to natural and synthetic HAp have shown, exclusively, the presence of the hexagonal crystalline phase, while only a few articles reported the probable presence of the monoclinic HAp. The monoclinic phase is thermodynamically more stable and mechanically superior to others, making it more appropriate for various medical applications. A similar finding was also reported by Morgan et al. who obtained the monoclinic HAp phase alongside the hexagonal phase on the specimen sintered at 900 °C [47].

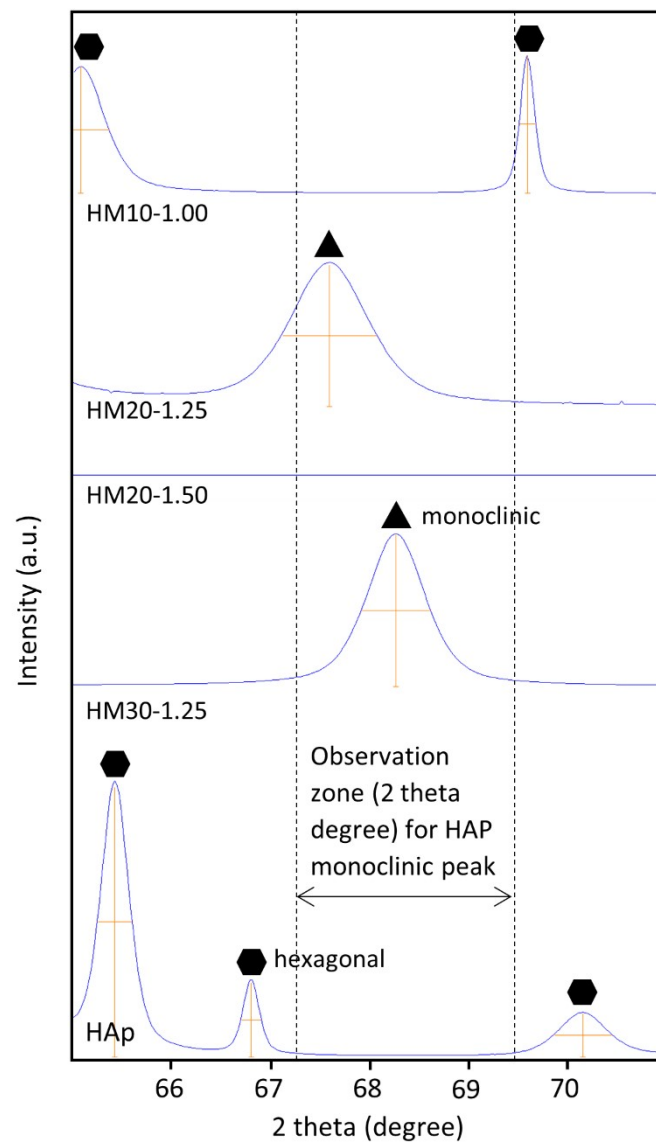


Figure 5. Magnified region at $65\text{--}71^\circ$ 2θ indicates a monoclinic peak observed within the range of 67° to 69° 2θ for HM20-1.25 and HM30-1.25.

Specifically, the specimen HM20 prepared at the 1.25 and 1.50 L/S ratios indicates the existence of the HAp phase alongside the calcium phosphate ($\text{Ca}_2\text{P}_2\text{O}_7$) crystalline phase (Powder Diffraction File—PDF No. 00-033-0297), and is considered as a byproduct of the chemical reaction [45], while other specimens indicate that the peak shifted when sintered at 900°C . The pattern in HM10-1.25, HM10-1.50, and HM20-1.00 indicates the presence of a well-crystallized structure belonging to sodium calcium phosphate silicate (PDF No. 00-033-1229) associated with the presence of the calcium phosphate byproduct, while HM30-1.50 shows the phase transformed to calcium hydrogen phosphate hydrate (Powder Diffraction File—PDF No. 00-011-0184) which may not be suitable for medical application especially in bone regeneration because of its lower C/P ratio of 1.33. These phase formations and phase transformations occurred due to the incomplete activation reaction during the initial preparation of the activated-HAp. This phenomenon refers to the situation where not all of the reactive silicate species were transformed into activated MK/HAp that might be contributed from chemical compositions of the metakaolin, activator, and HAp. Furthermore, the mix design input also influences the structural phase of the monoclinic and hexagonal hydroxyapatite as well as other phases.

3.2. Morphology

Figure 6 shows the scanning electron micrographs (SEM) of the selected mix design inputs of MK/HAp after sintering at 900 °C. The results indicated that the MK/HAp specimens with the highest added amount of metakaolin as shown in Figure 6c,d exhibited grain growth with a visible thick HAp neck formation. At this stage, pores were reduced and resulted in lower porosity compared to specimens in Figure 6a,b. The micrographs of the HM30 specimen clearly show the necking formation that occurred during sintering. On the other hand, the specimens with the lower added amount of metakaolin, which are HM10 (Figure 6a) and HM20 (Figure 6b), showed the development of grain boundaries and grain contact growth morphology with the presence of loosely packed particles. This suggests an initial stage of the sintering mechanism that was contributed by the incomplete densification of the specimens [48]. Thus, the micrograph proved that the sintering mechanism of the activated MK/HAp specimens can be achieved at a lower sintering temperature of 900 °C and this is in agreement with Noorina et al. in their study [31]. This was attributed to the chemical composition of the metakaolin as well as the alkali activator consisting of sodium and potassium which acted as a self-fluxing agent that lowered the sintering temperature, as reported by several previous studies [31,49,50]. This is a significant finding because much research on the sintering of the HAp observed that the optimized sintering temperature of the HAp ceramic can only be obtained within the range from 1150 °C to 1250 °C [24,51,52].

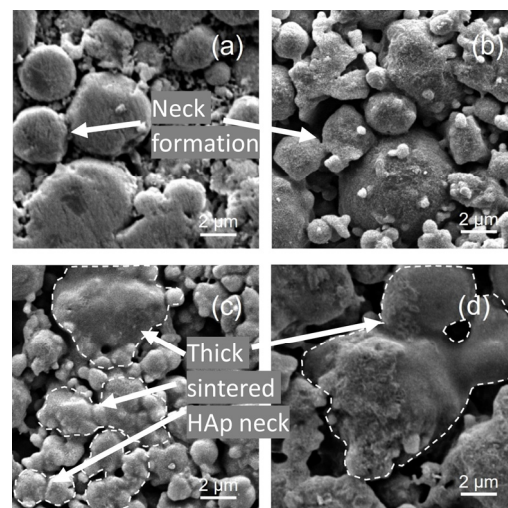


Figure 6. Micrographs of sintered MK/HAp ceramic specimens: (a) HM10-1.25, (b) HM20-1.00, (c) HM30-1.25 and (d) HM30-1.50.

3.3. Diametrical Tensile Strength (DTS) and Volume Shrinkage of MK/HAp Bio-Ceramic Body

Diametrical tensile strength (DTS), also known as the Brazilian method [53], offers the simplicity of testing brittle materials, in which the ultimate tensile strength of a brittle material is determined through compressive testing. The maximum tensile stress (σ_{\max}) along the diameter of the load, which was localized at the center of the specimens, decreased towards the periphery of the disc and changed its sign (compression). Only compressive stress existed in the vertical direction (y -axis) in which the magnitude became very great under the load. When the contact angle increases, the compressive stress can dramatically decrease. Therefore, failure may be initiated in the region with the higher compressive stress. Compressive stress induced tensile stress, perpendicular to the loaded diameter of the specimen, which is constant over a wide region around the center of the disc, and the rupture began at the point of maximum tensile strength. The specimen was then broken in two according to this diameter, as shown in Figure 7 [54].

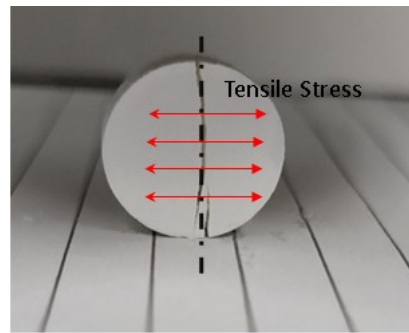


Figure 7. DTS Test.

Figure 8 represents the results of the (DTS) test conducted on all the specimens in conjunction with the as-sintered HAp ceramic as the control. As can be observed from the results, the strength of all MK/HAp specimens increased as the added amount of metakaolin increased. Meanwhile, the HAp ceramic sintered at 900 °C showed the lowest tensile strength.

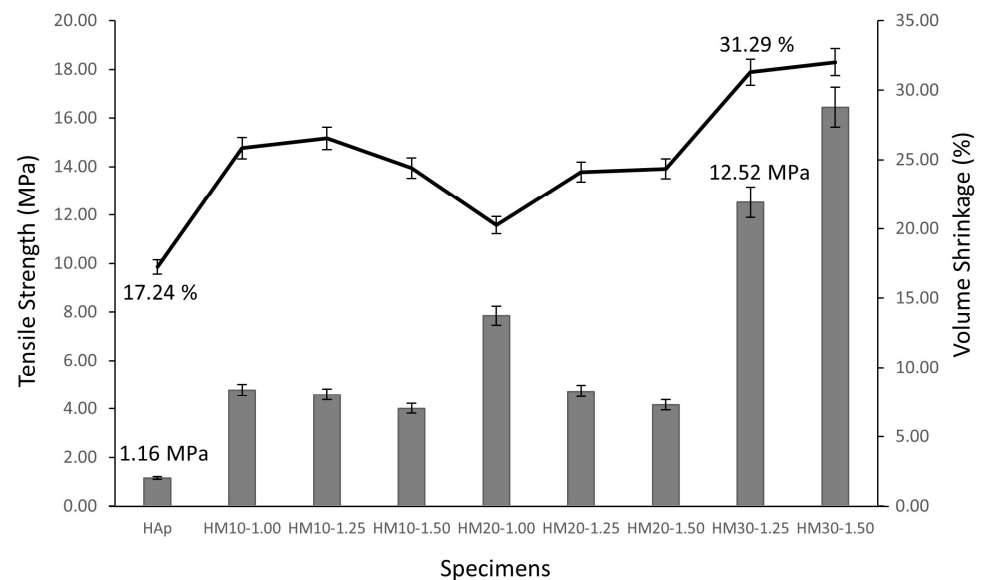


Figure 8. Diametral tensile strength (DTS) and the volume shrinkage of different mix design inputs of MK/HAp ceramics.

HM30-1.50 obtained the highest tensile strength of 16.5 MPa. However, this specimen did not exhibit the structural phase formation of hydroxyapatite (please refer to Figure 4), and thus it will not be further discussed in this paper. The specimen with the next highest tensile strength (12.5 MPa) and which recorded the formation of hydroxyapatite phase was HM30-1.25, which was initially prepared at the L/S ratio of 1.25. As discussed previously, HM30-1.25 was a unique specimen because it showed the formation of the monoclinic phase alongside the hexagonal phase, unlike others. This condition led to a significant increase in the strength due to the thermo-stable nature of the monoclinic structure. According to the study by Sanchez [45], compared to the HAp hexagonal phase, the monoclinic is thermodynamically more stable and provides better mechanical properties. Meanwhile, Obada [36] applied kaolin into the HAp to improve the mechano-biological properties of the bioceramic in which the material was found to be suitable for the human trabecular bone as the proposed scaffolds were endowed with an improved mechanical strength that matched the bearable range of the trabecular bone (2–12 MPa). Further to that, the contribution of the increased amount of metakaolin in the mixture to the increased strength is also in agreement with previous work [55]. This is because the composition of metakaolin

consisting of Al_2O_3 and SiO_2 species influenced the strength of the specimens. Furthermore, HM30-1.25, which exhibited complete densification, also contributed to a higher tensile strength (please refer to Figure 6). This can also be related to the higher volume shrinkage of the HM30-1.25 specimen due to the complete densification, where fewer pores can be observed in this specimen.

3.4. Thermogravimetric Analysis (TGA)

The thermogravimetric analysis (TGA) serves as an important tool for identifying the temperature at which organic substances are removed from the specimens. As can be observed from Figure 9, there was an 8% of weight loss of the HAp ceramics within the temperature range of 30 °C to 282 °C. The weight loss was attributed to the removal of incorporated water and moisture in the HAp ceramics. No significant weight loss was observed during the temperature rise to above 300 °C since no other substance was added to the specimens.

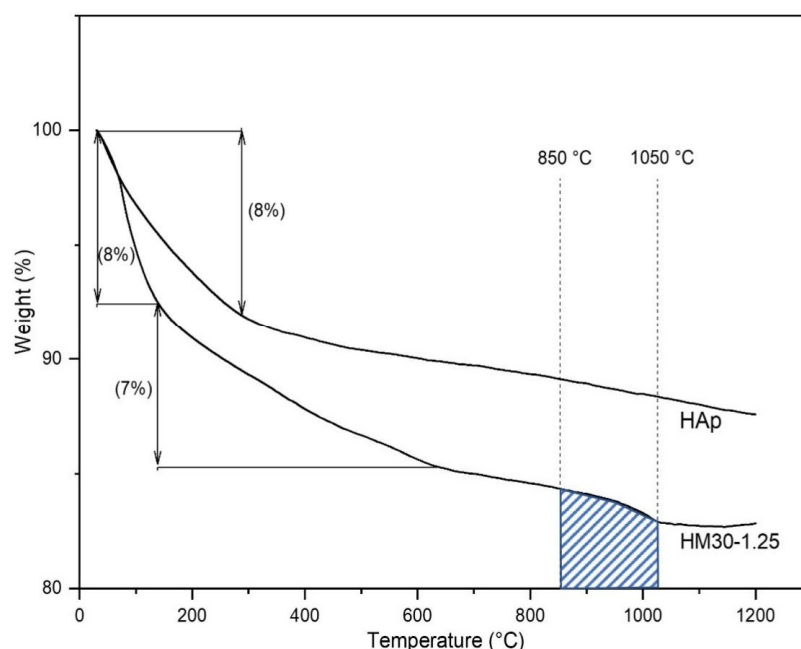


Figure 9. The TGA spectra of HAp and HM30-1.25 powder.

Meanwhile, a higher percentage of weight loss was observed for the HM30-1.25 specimen compared to the HAp. It was observed that the weight loss during thermal calcination in the temperature range of 30 to 630 °C occurred due to the removal of water (8%) and the binder substance (7%). Subsequently, a marginal weight loss curve was observed within the temperature range of 850 °C to 1050 °C. In this temperature range, metakaolin which is the source of aluminosilicate dissolved and resulted in weight loss. Thus, it can be concluded from the findings that the initial geopolymerization contributed to lowering the sintering temperature due to the absence of sodium from the alkali activator and metakaolin which acted as a self-fluxing agent. This was also reported in the previous work related to kaolin-GGBS geopolymer ceramics [31].

4. Conclusions

In this work, the effects of mix design inputs of MK/HAp on the formation of the hydroxyapatite phase and tensile strength were investigated. It was observed that the hydroxyapatite phase can be obtained from all the specimens, except for HM30 prepared at the L/S ratio of 1.5. Based on the study results, it can be concluded that the sintering temperature can be lowered to obtain the hydroxyapatite phase due to the resulting sodium and potassium from the alkali activator and metakaolin which also acted as a self-fluxing

agent. The XRD spectra of monoclinic and hexagonal structures were found in the HM30-1.25 specimen. The presence of the monoclinic phase in the HAp and the increased amount of metakaolin were found to increase the strength of the specimens.

Author Contributions: Conceptualization, W.M.A.W.I. and M.M.A.B.A.; methodology, W.M.A.W.I., N.H.J. and M.M.A.B.A.; software, W.M.A.W.I. and N.H.J.; validation M.M.A.B.A., M.A.A.M.S.; formal analysis, W.M.A.W.I., M.M.A.B.A., H.M. and N.H.J.; investigation, W.M.A.W.I., M.M.A.B.A., M.A.A.M.S., H.M., P.V., P.S. and N.H.J.; resources, W.M.A.W.I., N.H.J. and M.A.A.M.S.; data curation, W.M.A.W.I.; writing—original draft preparation W.M.A.W.I., M.M.A.B.A., M.S.B. and N.H.J.; writing—review and editing, M.M.A.B.A. and A.V.S.; visualization, W.M.A.W.I., M.M.A.B.A. and N.H.J.; supervision, M.M.A.B.A. and A.V.S.; project administration, W.M.A.W.I.; funding acquisition, M.M.A.B.A. All authors have read and agreed to the published version of the manuscript.

Funding: This research was funded by the Ministry of Higher Education, Malaysia, through the Fundamental Research Grant Scheme (FRGS) under reference number FRGS/1/2020/TK0/UNIMAP/01/2. This publication was supported by the Gheorghe Asachi Technical University of Iasi (TUIASI) from the University Scientific Research Fund (FCSU).

Institutional Review Board Statement: Not applicable.

Informed Consent Statement: Not applicable.

Data Availability Statement: Not applicable.

Acknowledgments: The authors gratefully acknowledge the financial support of the Centre of Excellence Geopolymer and Green Technology (CEGeoGTech), UniMAP. The authors also would like to extend their gratitude to the Ministry of Higher Education for sponsoring the Fundamental Research Grant Scheme (FRGS) FRGS/1/2020/TK0/UNIMAP/01/2. This research publication was supported by the Gheorghe Asachi Technical University of Iasi (TUIASI) from the University Scientific Research Fund (FCSU).

Conflicts of Interest: The authors declare that they have no known competing financial interest or personal relationships that could have appeared to influence the work reported in this paper.

References

1. Best, S.M.; Porter, A.E.; Thian, E.S.; Huang, J. Bioceramics: Past, present and for the future. *J. Eur. Ceram. Soc.* **2008**, *28*, 1319–1327. [[CrossRef](#)]
2. Shekhawat, D.; Singh, A.; Banerjee, M.K.; Singh, T.; Patnaik, A. Bioceramic composites for orthopaedic applications: A comprehensive review of mechanical, biological, and microstructural properties. *Ceram. Int.* **2021**, *47*, 3013–3030. [[CrossRef](#)]
3. Jeong, J.; Kim, J.H.; Shim, J.H.; Hwang, N.S.; Heo, C.Y. Bioactive calcium phosphate materials and applications in bone regeneration. *Biomater. Res.* **2019**, *23*, 4. [[CrossRef](#)] [[PubMed](#)]
4. Davaie, S.; Hooshmand, T.; Ansarifard, S. Different types of bioceramics as dental pulp capping materials: A systematic review. *Ceram. Int.* **2021**, *47*, 20781–20792. [[CrossRef](#)]
5. Cao, R.; Fang, Z.; Jin, M.; Shang, Y. Study on the Activity of Metakaolin Produced by Traditional Rotary Kiln in China. *Minerals* **2022**, *12*, 365. [[CrossRef](#)]
6. Broda, E.; Skwarek, E. Clay, Hydroxyapatite and Their Composites—Brief Review. In *Nanooptics and Photonics, Nanochemistry and Nanobiotechnology, and Their Applications, Proceedings of the 7th International Conference Nanotechnology and Nanomaterials (NANO2019), Lviv, Ukraine, 27–30 August 2019*; pp. 255–272. [[CrossRef](#)]
7. Biedrzycka, A.; Skwarek, E.; Hanna, U.M. Hydroxyapatite with magnetic core: Synthesis methods, properties, adsorption and medical applications. *Adv. Colloid Interface Sci.* **2021**, *291*, 102401. [[CrossRef](#)]
8. Arokiasamy, P.; Abdullah, M.M.A.B.; Rahim, S.Z.A.; Luhar, S.; Sandu, A.V.; Jamil, N.H.; Nabiałek, M. Synthesis methods of hydroxyapatite from natural sources: A review. *Ceram. Int.* **2022**, *48*, 14959–14979. [[CrossRef](#)]
9. Mardziah, C.M.; Ramesh, S.; Wahid, M.A.; Chandran, H.; Sidhu, A.; Krishnasamy, S.; Purbolaksono, J. Effect of zinc ions on the structural characteristics of hydroxyapatite bioceramics. *Ceram. Int.* **2020**, *46*, 13945–13952. [[CrossRef](#)]
10. Salman, S.; Gunduz, O.; Yilmaz, S.; Öveçoğlu, M.; Snyder, R.L.; Agathopoulos, S.; Oktar, F. Sintering effect on mechanical properties of composites of natural hydroxyapatites and titanium. *Ceram. Int.* **2009**, *35*, 2965–2971. [[CrossRef](#)]
11. Broda, E.; Skwarek, E.; Payentko, V.V.; Gunko, V.M. Synthesis and selected physicochemical properties of hydroxyapatite and white clay composite. *Physicochem. Probl. Miner. Process.* **2019**, *55*, 1475–1483. [[CrossRef](#)]
12. Hübner, W.; Blume, A.; Pushnjakova, R.; Dekhtyar, Y.; Hein, H.-J. The Influence of X-ray Radiation on the Mineral/Organic Matrix Interaction of Bone Tissue: An FT-IR Microscopic Investigation. *Int. J. Artif. Organs* **2005**, *28*, 66–73. [[CrossRef](#)]

13. Bystrova, A.V.; Dekhtyar, Y.D.; Popov, A.I.; Coutinho, J.; Bystrov, V.S. Modified Hydroxyapatite Structure and Properties: Modeling and Synchrotron Data Analysis of Modified Hydroxyapatite Structure. *Ferroelectrics* **2015**, *475*, 135–147. [[CrossRef](#)]
14. Kroczek, K.; Turek, P.; Mazur, D.; Szczygielski, J.; Filip, D.; Brodowski, R.; Balawender, K.; Przeszłowski, Ł.; Lewandowski, B.; Orkisz, S.; et al. Characterisation of Selected Materials in Medical Applications. *Polymers* **2022**, *14*, 1526. [[CrossRef](#)]
15. Hou, X.; Zhang, L.; Zhou, Z.; Luo, X.; Wang, T.; Zhao, X.; Lu, B.; Chen, F.; Zheng, L. Calcium Phosphate-Based Biomaterials for Bone Repair. *J. Funct. Biomater.* **2022**, *13*, 187. [[CrossRef](#)] [[PubMed](#)]
16. Tavoni, M.; Dapporto, M.; Tampieri, A.; Sprio, S. Bioactive calcium phosphate-based composites for bone regeneration. *J. Compos. Sci.* **2021**, *5*, 227. [[CrossRef](#)]
17. Ielo, I.; Calabrese, G.; de Luca, G.; Conoci, S. Recent Advances in Hydroxyapatite-Based Biocomposites for Bone Tissue Regeneration in Orthopedics. *Int. J. Mol. Sci.* **2022**, *23*, 9721. [[CrossRef](#)] [[PubMed](#)]
18. de Lama-Odría, M.d.C.; del Valle, L.J.; Puiggalí, J. Hydroxyapatite Biobased Materials for Treatment and Diagnosis of Cancer. *Int. J. Mol. Sci.* **2022**, *23*, 11352. [[CrossRef](#)]
19. Kargozar, S.; Mollazadeh, S.; Kermani, F.; Webster, T.J.; Nazarnezhad, S.; Hamzehlou, S.; Baino, F. Hydroxyapatite Nanoparticles for Improved Cancer Theranostics. *J. Funct. Biomater.* **2022**, *13*, 100. [[CrossRef](#)]
20. Lara-Ochoa, S.; Ortega-Lara, W.; Guerrero-Beltrán, C.E. Hydroxyapatite nanoparticles in drug delivery: Physicochemistry and applications. *Pharmaceutics* **2021**, *13*, 1642. [[CrossRef](#)] [[PubMed](#)]
21. Carella, F.; Degli Esposti, L.; Adamiano, A.; Iafisco, M. The use of calcium phosphates in cosmetics, state of the art and future perspectives. *Materials* **2021**, *14*, 6398. [[CrossRef](#)]
22. Chen, L.; Al-Bayatee, S.; Khurshid, Z.; Shavandi, A.; Brunton, P.; Ratnayake, J. Hydroxyapatite in oral care products—A review. *Materials* **2021**, *14*, 4865. [[CrossRef](#)] [[PubMed](#)]
23. Obada, D.O.; Dauda, E.T.; Abifarin, J.K.; Dodoo-Arhin, D.; Bansod, N.D. Mechanical properties of natural hydroxyapatite using low cold compaction pressure: Effect of sintering temperature. *Mater. Chem. Phys.* **2020**, *239*, 122099. [[CrossRef](#)]
24. Champion, E. Sintering of calcium phosphate bioceramics. *Acta Biomater.* **2013**, *9*, 5855–5875. [[CrossRef](#)] [[PubMed](#)]
25. Kim, H.T.; Han, J.S.; Yang, J.H.; Lee, J.B.; Kim, S.H. The effect of low temperature aging on the mechanical property & phase stability of Y-TZP ceramics. *J. Adv. Prosthodont.* **2009**, *1*, 113–117. [[CrossRef](#)] [[PubMed](#)]
26. Indurkar, A.; Choudhary, R.; Rubenis, K.; Locs, J. Advances in sintering techniques for calcium phosphates ceramics. *Materials* **2021**, *14*, 6133. [[CrossRef](#)]
27. Puajindanetr, S.; Best, S.M.; Bonfield, W. Characterization and sintering of precipitated hydroxyapatite. *Br. Ceram. Trans.* **1994**, *93*, 96–99.
28. Aarthy, S.; Thenmuhil, D.; Dharunya, G.; Manohar, P. Exploring the effect of sintering temperature on naturally derived hydroxyapatite for bio-medical applications. *J. Mater. Sci. Mater. Med.* **2019**, *30*, 21. [[CrossRef](#)] [[PubMed](#)]
29. Ou, S.F.; Chiou, S.Y.; Ou, K.L. Phase transformation on hydroxyapatite decomposition. *Ceram. Int.* **2013**, *39*, 3809–3816. [[CrossRef](#)]
30. Ruys, A.J.; Wei, M.; Sorrell, C.C.; Dickson, M.R.; Brandwoods, A.; Milthomes, B.K. Sintering effects on the strength hydroxyapatite of hydroxyapatite. *Biomaterials* **1995**, *16*, 409–415. [[CrossRef](#)]
31. Jamil, N.H.; Abdullah, M.; Pa, F.; Mohamad, H.; Ibrahim, W.; Amonpattaratkit, P.; Gondro, J.; Sochacki, W.; Ibrahim, N. Self-fluxing mechanism in geopolymerization for low-sintering temperature of ceramic. *Materials* **2021**, *14*, 1325. [[CrossRef](#)]
32. Catauro, M.; Bollino, F.; Papale, F.; Lamanna, G. Investigation of the sample preparation and curing treatment effects on mechanical properties and bioactivity of silica rich metakaolin geopolymer. *Mater. Sci. Eng. C* **2014**, *36*, 20–24. [[CrossRef](#)]
33. Sunendar, B.; Fathina, A.; Harmaji, A.; Mardhian, D.F.; Asri, L.; Widodo, H.B. The effect of CHA-doped Sr addition to the mechanical strength of metakaolin dental implant geopolymer composite. *AIP Conf. Proc.* **2017**, *1887*, 020020. [[CrossRef](#)]
34. Kaze, C.R.; Jiofack, S.B.K.; Cengiz, Ö.; Alomayri, T.S.; Adesina, A.; Rahier, H. Reactivity and mechanical performance of geopolymer binders from metakaolin/meta-halloysite blends. *Constr. Build. Mater.* **2022**, *336*, 127546. [[CrossRef](#)]
35. Costa, L.M.; Almeida, N.G.S.; Houmard, M.; Cetlin, P.R.; Silva, G.J.B.; Aguilar, M.T.P. Influence of the addition of amorphous and crystalline silica on the structural properties of metakaolin-based geopolymers. *Appl. Clay Sci.* **2021**, *215*, 106312. [[CrossRef](#)]
36. Obada, D.O.; Osseni, S.A.; Sina, H.; Salami, K.A.; Oyedeji, A.N.; Dodoo-Arhin, D.; Bansod, N.D.; Csaki, S.; Atta, A.Y.; Fasanya, O.O.; et al. Fabrication of novel kaolin-reinforced hydroxyapatite scaffolds with robust compressive strengths for bone regeneration. *Appl. Clay Sci.* **2021**, *215*, 106298. [[CrossRef](#)]
37. Liu, X.; Jiang, J.; Zhang, H.; Li, M.; Wu, Y.; Guo, L.; Wang, W.; Duan, P.; Zhang, W.; Zhang, Z. Thermal stability and microstructure of metakaolin-based geopolymer blended with rice husk ash. *Appl. Clay Sci.* **2020**, *196*, 105769. [[CrossRef](#)]
38. Hsieh, Y.C.; Lee, W.H.; Liao, P.H. Using geopolymer technology on synthesizing leucite ceramics. *Polymers* **2021**, *13*, 3621. [[CrossRef](#)] [[PubMed](#)]
39. Ahmad, R.; Ibrahim, W.M.W.; Abdullah, M.M.A.B.; Pakawanit, P.; Vizureanu, P.; Abdullah, A.S.; Sandu, A.V.; Zaidi, F.H.A. Geopolymer-Based Nepheline Ceramics: Effect of Sintering Profile on Morphological Characteristics and Flexural Strength. *Crystals* **2022**, *12*, 1313. [[CrossRef](#)]
40. Kenne Dikko, B.B.; Elimbi, A.; Cyr, M.; Dika Manga, J.; Tchakoute Kouamo, H. Effect of the rate of calcination of kaolin on the properties of metakaolin-based geopolymers. *J. Asian Ceram. Soc.* **2015**, *3*, 130–138. [[CrossRef](#)]
41. Tchakouté, H.K.; Fotio, D.; Rüscher, C.H.; Kamseu, E.; Djobo, J.N.; Bignozzi, M.C.; Leonelli, C. The effects of synthesized calcium phosphate compounds on the mechanical and microstructural properties of metakaolin-based geopolymer cements. *Constr. Build. Mater.* **2018**, *163*, 776–792. [[CrossRef](#)]

42. Kim, B.; Lee, S.; Chon, C.M.; Cho, S. Setting Behavior and Phase Evolution on Heat Treatment of Metakaolin-Based Geopolymers Containing Calcium Hydroxide. *Materials* **2022**, *15*, 194. [[CrossRef](#)] [[PubMed](#)]
43. Rubenis, K.; Zemjane, S.; Vecstaudza, J.; Biteniaks, J.; Locs, J. Densification of amorphous calcium phosphate using principles of the cold sintering process. *J. Eur. Ceram. Soc.* **2021**, *41*, 912–919. [[CrossRef](#)]
44. Jurgelane, I.; Buss, A.; Putnina, M.; Loca, D.; Locs, J. Effect of sintering temperature on sorption properties and compressive strength of calcium phosphate ceramic granules. *Mater. Lett.* **2021**, *282*, 128858. [[CrossRef](#)]
45. Sánchez-campos, D.; Valderrama, M.R.; López-Ortiz, S.; Salado-Leza, D.; Fernández-García, M.; Mendoza-Anaya, D.; Salinas-Rodríguez, E.; Rodríguez-Lugo, V. Modulated monoclinic hydroxyapatite: The effect of pH in the microwave assisted method. *Minerals* **2021**, *11*, 314. [[CrossRef](#)]
46. Ma, G.; Liu, X.Y. Hydroxyapatite: Hexagonal or monoclinic? *Cryst. Growth Des.* **2009**, *9*, 2991–2994. [[CrossRef](#)]
47. Morgan, H.; Wilson, R.M.; Elliott, J.C.; Dowker, S.E.P.; Anderson, P. Preparation and characterisation of monoclinic hydroxyapatite and its precipitated carbonate apatite intermediate. *Biomaterials* **2000**, *21*, 617–627. [[CrossRef](#)]
48. Chen, P.Y.; Wang, S.-F.; Chien, R.; Tu, C.-S.; Feng, K.-C.; Chen, C.-S.; Hung, K.-Y.; Schmidt, V.H. Evolution of the microstructural and mechanical properties of hydroxyapatite bioceramics with varying sintering temperature. *Ceram. Int.* **2019**, *45*, 16226–16233. [[CrossRef](#)]
49. Jamil, N.H.; Abdullah, M.M.A.B.; Che Pa, F.; Mohamad, H.; Ibrahim, W.M.A.W.; Chaiprapa, J. Influences of SiO₂, Al₂O₃, CaO and MgO in phase transformation of sintered kaolin-ground granulated blast furnace slag geopolymer. *J. Mater. Res. Technol.* **2020**, *9*, 14922–14932. [[CrossRef](#)]
50. ter Teo, P.; Anasyida, A.S.; Kho, C.M.; Nurulakmal, M.S. Recycling of Malaysia's EAF steel slag waste as novel fluxing agent in green ceramic tile production: Sintering mechanism and leaching assessment. *J. Clean. Prod.* **2019**, *241*, 118144. [[CrossRef](#)]
51. Khamkongkao, A.; Boonchuduang, T.; Klysubun, W.; Amonpattaratkit, P.; Chunate, H.-T.; Tuchinda, N.; Pimsawat, A.; Daengsakul, S.; Suksangrat, P.; Sailuam, W.; et al. Sintering behavior and mechanical properties of hydroxyapatite ceramics prepared from Nile Tilapia (*Oreochromis niloticus*) bone and commercial powder for biomedical applications. *Ceram. Int.* **2021**, *47*, 34575–34584. [[CrossRef](#)]
52. Ramesh, S.; Aw, K.; Tolouei, R.; Amiriyan, M.; Tan, C.; Hamdi, M.; Purbolaksono, J.; Hassan, M.; Teng, W. Sintering properties of hydroxyapatite powders prepared using different methods. *Ceram. Int.* **2013**, *39*, 111–119. [[CrossRef](#)]
53. Abdulsameea, N.; Hassaan, M.Y.; Rashed, O.; Soliman, I.E.; Tiama, T.M. Effect of Oxygen Plasma Treatment on Some Physical Properties of Nanoparticles Glass Ionomer Cement Doped With ZnO or TiO₂. *EC Dent. Sci.* **2017**, *13*, 24–38.
54. Es-saddik, M.; Laasri, S.; Laghzizil, A.; Guidara, A.; Chaari, K.; Bouaziz, J.; Banouni, H.; Hajjaji, A.; Taha, M. The densification and diametral compression strength of Hydroxyapatite-Zirconia bioceramics: Experimental and modelling studies. *Mater. Today Proc.* **2022**, *52*, 71–77. [[CrossRef](#)]
55. Jithendra, C.; Dalawai, V.N.; Elavenil, S. Effects of metakaolin and sodium silicate solution on workability and compressive strength of sustainable Geopolymer mortar. *Mater. Today Proc.* **2022**, *51*, 1580–1584. [[CrossRef](#)]

Disclaimer/Publisher's Note: The statements, opinions and data contained in all publications are solely those of the individual author(s) and contributor(s) and not of MDPI and/or the editor(s). MDPI and/or the editor(s) disclaim responsibility for any injury to people or property resulting from any ideas, methods, instructions or products referred to in the content.